

Characteristics of radiative events in deep inelastic ep scattering at HERA

A. Kwiatkowski¹, H. Spiesberger^{1,*} and H.-J. Möhring²

¹ II. Institut für Theoretische Physik der Universität Hamburg, Luruper Chaussee 149, W-2000 Hamburg 50, Federal Republic of Germany

² Sektion Physik, Universität Leipzig, Karl-Marx-Platz 10–11, O-7010 Leipzig, Federal Republic of Germany

Received 23 November 1990

Abstract. A major contribution to the electroweak radiative corrections in deep inelastic electron proton scattering is due to hard photon bremsstrahlung $ep \rightarrow e\gamma X$. The Monte Carlo event generator HERACLES is used to study this process. Predictions for event distributions are given and the observability of radiative events is discussed. As a result we find that cuts can be found that reduce the radiative corrections considerably.

1 Introduction

In order to plan the deep inelastic electron proton scattering experiments at HERA it is necessary to have detailed information on the characteristics of events that are predicted by the standard theory. Higher order electroweak effects not only change the amplitudes of the tree graph processes, but in order to describe higher order corrections consistently one has also to consider the process with additional photons. The most flexible method to study these effects is by the use of a Monte Carlo event generator which simulates an experiment by constructing events according to probabilities given by the appropriate differential cross sections. Samples of generated events can then easily be used to perform simulations of measurements that one might imagine to be of interest.

Radiative corrections to the differential cross section $d^2\sigma/dx dy$ for deep inelastic electron proton scattering and numerical results for HERA energies have been calculated in [1–3] for the neutral current and in [4, 5] for the charged current (see also [6]). These calculations used analytic and numerical integration techniques and treated the photon totally inclusive, i.e. no restrictions on the phase space of the bremsstrahlung photon have been imposed. The results obtained there for the leptonic contributions have been confirmed by calculations based on the collinear approximation in [7, 8]. Monte Carlo approaches have been used in [9] for the $\mathcal{O}(\alpha)$ leptonic radiation in the collinear approximation and in [10] for

the bremsstrahlung in small angle elastic scattering $ep \rightarrow ep\gamma$. A Monte Carlo integration technique has also been used in [11] for the calculation of the charged current radiative corrections. The methods introduced in [11] were the starting point for the development of the Monte Carlo event generator HERACLES for the simulation of deep inelastic ep collisions via the neutral current interactions at HERA including electroweak radiative effects [12].

In this paper we present first results obtained with the help of the event generator HERACLES. After a short description of the program and the physics simulated by it in Sects. 2 and 3 we are going to compare the results obtained from HERACLES with results of other calculations [1, 3] (Sect. 4). We will then discuss the distribution of events to be expected at HERA with respect to energies and angles of the outgoing particles (scattered electrons, quarks, and photons) in Sect. 5.

The knowledge of the detailed features of radiative events will lead us to an understanding of the origin of the large radiative corrections. We will show that these large corrections are due to hard photon emission. Hard photons are potentially visible in the detector and the study of their angular distribution will allow to answer the question whether radiative events could be identified experimentally. If these events are excluded from the data sample used for a physics analysis, the remaining corrections which are due to unidentified radiative events would be smaller. This is important if one of the standard unfolding algorithms [13] shall be used because they can deal with corrections of moderate size only. After cutting out radiative events these unfolding procedures could be applied over a larger range of x and y than one could have expected from a study of the fully inclusive bremsstrahlung corrections. In Sect. 6 we will show the effect of several simplified cuts on the radiative corrections and discuss their experimental feasibility.

2 Description of the event generator HERACLES

The first order electroweak radiative corrections to deep inelastic scattering at HERA are known to be large, par-

* Supported by Bundesministerium für Forschung und Technologie, 055HH91P(8), Bonn, FRG

ticularly in the low- x /high- y region [1, 2]. They are dominated by contributions describing the radiation of real and virtual photons from the lepton line. These leptonic corrections together with the fermionic contributions to the photon and Z self energies (see Fig. 1) are sufficient to describe the differential cross section $d^2\sigma/dx dy$ with an accuracy of better than 5% if Q^2 is not extremely large. For smaller Q^2 , (below $2 \times 10^3 \text{ GeV}^2$) the neglected corrections are even below 1%. A classification of the complete electroweak corrections of $\mathcal{O}(\alpha)$ and their discussion has been given e.g. in [3].

The event generator HERACLES includes the leptonic corrections as well as the complete one-loop virtual corrections and is thus able to give a good description of the neutral current reaction at HERA including radiative effects. Explicit formulas for the corrections contained in HERACLES can be found in [2].

The most important capabilities of the generator are:

- It allows integration of the differential cross sections for $ep \rightarrow eX$ and $ep \rightarrow e\gamma X$ over kinematical regions which can be defined in terms of the variables x , y , Q^2 , which are determined from the outgoing electron's energy and scattering angle. As well, in the calculation of the cross section for $ep \rightarrow e\gamma X$ it is possible to limit the phase space by requiring a minimal value for the photon energy E_γ .
- The program performs event generation in predefined kinematical regions, as in the integration step. The generated events are described by the 4-momenta of the final state particles (electrons, quarks, and photons) and the flavor of the scattered quark.
- The structure of the program allows a separate treatment of the Born term and three parts of the leptonic photonic corrections (comprising soft and hard leptonic bremsstrahlung and the corresponding virtual corrections). These parts describe initial state radiation, final state radiation, and a contribution called Compton part.
- Optionally, various parts of weak virtual corrections can be included (self energies, vertex corrections, box diagrams).
- The program describes electron as well as positron scattering and allows for polarized leptons.
- The user can choose among a set of parametrizations for input parton distributions. The list of parametrizations may be easily extended by the user.

The present version 2.1 of the generator is, however, not yet complete. The following aspects of ep physics cannot yet be investigated with the help of HERACLES:

- 1) The hadronic final state is not generated but the simulation is done at the parton level only. Therefore also no QCD corrections are included which could e.g. lead to the appearance of two-jet events.

- 2) Only the neutral current reaction but not the charged current is included.
- 3) Radiation from the quark line and lepton-quark interference contributions to virtual and real bremsstrahlung are not yet implemented.
- 4) The radiative tails from elastic and quasielastic scattering are not included.

We plan to complete step by step the Monte Carlo generator and build in the missing pieces.

There are several restrictions to the (x, y) region where the program in the present version works reliably: As long as exponentiation of soft photonic corrections is not included, the applicability of the program will be restricted to not too small values of y and not too large x where the non-radiative part of the corrections can become small and even negative. In the present version x and y must lie in the region

$$y(1-x)^2 \geq 0.004.$$

In addition, the value of the momentum transfer Q^2 is restricted to be bigger than 4 GeV^2 . For small values of Q^2 the basic parton model assumption becomes invalid and a formulation of the radiative corrections on the basis of structure functions is needed.

The results of HERACLES have been compared with those of other programs where the photon was integrated out completely. We will discuss this comparison in some more detail in Sect. 4. The comparison has shown good agreement in the range

$$10^{-3} \leq x \leq 0.9, \\ 0.02 \leq y \leq 0.95.$$

The computational techniques applied in HERACLES are based on the methods used in the AXO library [14] for Monte Carlo integration and event generation. AXO itself and the integration routine VEGAS contained in it relies on the Monte Carlo integration algorithm by P. Lepage [15]. For further technical details we refer the reader to the HERACLES user manual [12] and to [16].

3 Monte Carlo treatment of radiative corrections

The characteristic behaviour of the leptonic corrections is governed by the collinear peaks coming from initial and final state radiation. After integration over the photon phase space they lead to large logarithms $\ln(Q^2/m_e^2)$. In addition to them, as a peculiarity for t -channel processes, the $1/Q^2$ pole of the photon propagator can lead to a strong distortion of the simple bremsstrahlung cross section: emission of photons with momentum k shifts

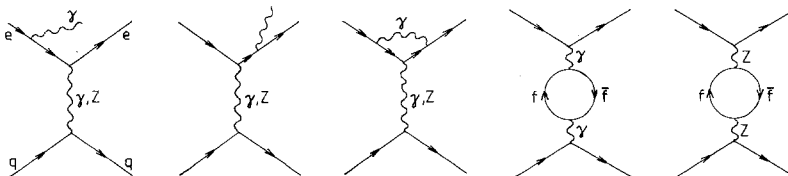


Fig. 1. Feynman diagrams describing the $\mathcal{O}(\alpha)$ leptonic corrections for neutral current electron quark scattering and the fermionic contributions to the photon and Z self energies

the momentum transfer $Q^2 = -(p_e - p'_e)^2$ measured from the momenta of the incoming (p_e) and outgoing electron (p'_e) to $\hat{Q}^2 = -(p_e - p'_e - k)^2$. Since \hat{Q}^2 can be very small as compared to Q^2 this can lead to a strong enhancement of the radiative cross section similar to the radiative tail effect above a resonance. The enhancement is especially important for hard initial state radiation where the bremsstrahlung photon is emitted along the direction of the incoming electron. But it also leads to a large cross section for events where the photon balances the transverse momentum of the scattered electron such that \hat{Q}^2 becomes small.

Due to the complicated peaking behaviour, the complete cross section cannot be simulated directly. To simplify the problem we have split the complete cross section into several parts whose peaking behaviour is determined by only one kinematical variable. After that, simple transformations of the variables can be found that render the integrands flat. In the following we discuss this separation and the characteristics of the resulting parts (called "channels" in the Monte Carlo). Details of the cross section formulas are given in the appendix.

The first contribution, called *non-radiative channel*, contains the Born cross section and virtual as well as soft real $\mathcal{O}(\alpha)$ corrections. Events generated in this channel contain two particles in the final state namely the scattered electron and the outgoing quark. These events are thus completely described by two kinematical variables which can be e.g. two of the following:

$$\begin{aligned} Q^2 &= -(p_e - p'_e)^2, \\ x &= \frac{Q^2}{2P(p_e - p'_e)}, \\ y &= \frac{P(p_e - p'_e)}{Pp_e} = \frac{Q^2}{xS}, \end{aligned} \quad (1)$$

where $S = (p_e + P)^2$ and the meaning of the momenta is indicated in Fig. 2. These variables are determined from the momentum of the scattered electron. It is also possible to rewrite the definition of x , y , and Q^2 with the help of the momentum of the hadronic final state which is of experimental relevance for charged current scattering and for the neutral current process in a certain kinematical range [17]. For radiative events these two ways of determining the kinematical variables from experimentally measured momenta will lead to different results if the photon momentum is not included in the total momentum of the hadronic final state. In the following we will always use the definitions (1), also in the case of radiative events.

In order to simulate the lowest order cross section effectively we have actually chosen x and $g = -1/Q^2$ as variables. The variable g was chosen in order to get rid of the dominating Q^2 dependence coming from the photon exchange propagator.

The soft photon corrections contained in the non-radiative channel are the result of an analytic integration over a small region in the phase space around the infrared singular point $E_\gamma = 0$. The separation of this soft part is defined with the help of a maximal photon energy k_0 . The cutoff k_0 is chosen to be small as compared to the energies of the fermions such that the soft photon approximation is justified and an analytical treatment of the phase space integration is possible. The contribution of the non-radiative channel consequently depends on the unphysical parameter k_0 . But this dependence on k_0 will disappear when photons of energies bigger than k_0 are included. These hard photon contributions are contained in the radiative channels. In the numerical evaluation k_0 is chosen smaller than the experimental resolution for photon detection. The soft bremsstrahlung thus describes the emission of unobservable photons and its inclusion in the non-radiative part is justified.

In order to describe the treatment of the *radiative channels* we concentrate on the pure photon exchange contribution to the cross section which is essentially determined by the factor

$$\frac{1}{z_1 z_2 \hat{Q}^2},$$

with $z_1 = 2(k \cdot p_e)$, $z_2 = 2(k \cdot p'_e)$ (see (30) of the appendix). The factors in the denominator are not independent from each other, they obey the relation

$$\hat{Q}^2 = -(p_e - p_e' - k)^2 = Q^2 + z_1 - z_2. \quad (2)$$

A partial fractioning leads to a separation of the singularities:

$$\begin{aligned} \frac{1}{z_1 z_2 \hat{Q}^2} &= \frac{1}{z_1} \frac{1}{z_1 + z_2 + \hat{Q}^2} \left(\frac{1}{z_1 + z_2} + \frac{1}{z_1 + \hat{Q}^2} \right) \\ &+ \frac{1}{z_2} \frac{1}{z_1 + z_2 + \hat{Q}^2} \left(\frac{1}{z_1 + z_2} + \frac{1}{z_2 + \hat{Q}^2} \right) \\ &+ \frac{1}{\hat{Q}^2} \frac{1}{z_1 + z_2 + \hat{Q}^2} \left(\frac{1}{z_1 + \hat{Q}^2} + \frac{1}{z_2 + \hat{Q}^2} \right). \end{aligned} \quad (3)$$

It is important to note that the factors multiplying the pole terms $1/z_1$, $1/z_2$, and $1/\hat{Q}^2$ do not vary strongly and for kinematically allowed configurations none of the other denominators can become small. Using this, the cross section can be decomposed into the form

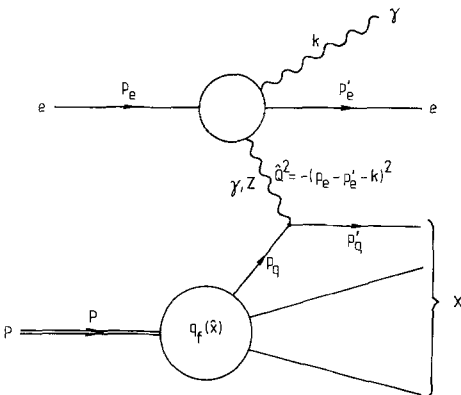


Fig. 2. Notations for deep inelastic lepton proton scattering in the parton model

$$\frac{d^5\sigma}{dx dy d^3\mathbf{k}} = \frac{M_1}{z_1} + \frac{M_2}{z_2} + \frac{M_{\hat{Q}^2}}{\hat{Q}^2}. \quad (4)$$

This separation defines three radiative channels:

- initial state radiation, peaking for $z_1 \rightarrow 0$, i.e. for events where the photon is emitted collinearly with the incoming electron,
- final state radiation, peaking for $z_2 \rightarrow 0$, i.e. for events where the photon is emitted collinearly with the scattered electron, and
- Compton part, peaking for $\hat{Q}^2 \rightarrow 0$. The condition $\hat{Q}^2 = 0$ fixes the energy and the emission angle of the photon as functions of x and y :

$$\begin{aligned} E_\gamma^C &= yE_e + x(1-y)E_p, \\ \cos\theta_\gamma^C &= \frac{yE_e - x(1-y)E_p}{yE_e + x(1-y)E_p}. \end{aligned} \quad (5)$$

(E_e and E_p are the energies of the incoming electron and of the proton and fermion masses have been neglected here). These expressions are identical to the relations determining the energy $E_{q'}$ and the angle $\theta_{q'}$ of the final quark from x and y in the case of non-radiative scattering, i.e. for the $2 \rightarrow 2$ process $eq_f \rightarrow eq_f$. From (5) one finds for the transverse momentum of the photon

$$k_T^C = E_\gamma^C \sin\theta_\gamma^C = 2\sqrt{xy(1-y)} E_e E_p, \quad (6)$$

and k_T^C turns out to be equal to the electron transverse momentum

$$k_T^C = p'_{e,T}. \quad (7)$$

The events favored by this fourth channel are thus characterized by a photon balancing the transverse momentum of the scattered electron and a final quark that is going close to the initial quark direction. This third contribution to the bremsstrahlung cross section is called the Compton part because it can be viewed as resulting from the emission of a quasireal photon from the quark line with subsequent Compton scattering $e\gamma \rightarrow e\gamma$.

After this separation one can use simple variable transformations to map the various contributions to the cross section onto flat functions. One of the substitutions

$$z_1 \rightarrow \ln z_1, \quad z_2 \rightarrow \ln z_2, \quad \hat{Q}^2 \rightarrow \ln \hat{Q}^2 \quad (8)$$

in each channel is sufficient to get rid of the pole factors in (4). We found that the same prescriptions are also sufficient for the double pole contributions in (30) of the appendix which are proportional to

$$\frac{m_e^2}{(kp_e)^2}, \quad \frac{m_e^2}{(kp'_e)^2}.$$

They are separated similarly using

$$\frac{1}{z_i^2 \hat{Q}^4} = \frac{1}{z_i^2} \frac{1}{z_i^2 + \hat{Q}^4} + \frac{1}{\hat{Q}^4} \frac{1}{z_i^2 + \hat{Q}^4}. \quad (9)$$

At first sight one would guess that substitutions $z_i \rightarrow 1/z_i$ and $\hat{Q}^2 \rightarrow 1/\hat{Q}^2$ are necessary. We have checked that us-

ing these transformations and treating the double pole parts separately leads to the same results as the prescriptions (8). Therefore the double pole parts are included in the corresponding channels.

The separation into three radiative channels was exemplified with the help of the photon exchange contribution to the cross section. The photon- Z boson interference and the Z boson exchange parts are treated similarly, except that for them there is no contribution to the Compton channel.

The treatment of the Compton part deserves some further discussion. After integration over the photon phase space the $1/\hat{Q}^2$ singularity leads to the appearance of logarithms $\ln Q^2/\hat{Q}_{\min}^2$ where \hat{Q}_{\min}^2 is determined by the mass assigned to the hadronic state. In a parton model calculation this would be a quark mass which makes the result depending on an unphysical parameter. As is the case for contributions from quarkonic radiation, this mass singular part has to be absorbed into the hadronic structure functions. In order to do this one has to generalize the parton model relation which expresses the structure functions in terms of quark distributions and allow for a contribution $D_{\gamma/P}(x, \hat{Q}^2)$ describing the photon content inside a proton (see [8, 18] for details). For large momentum transfers, $D_{\gamma/P}$ can be derived from the quark distribution functions, but at small \hat{Q}^2 one expects that non-perturbative contributions are important. A correct treatment would start with a formulation of the radiative corrections with the help of structure functions of the hadronic tensor which does not rely on the parton model. This is indeed possible for the $\mathcal{O}(\alpha)$ leptonic corrections. For a numerical evaluation of the corrections one can then use parametrizations of the structure functions which describe not only the deep inelastic region but also the low \hat{Q}^2 range correctly. In this work we did not follow this line but instead used naively the parton model expressions for the structure functions. In order to compare the Monte Carlo results with former calculations we present results where the Duke-Owens parametrizations were used down to values of the momentum transfer \hat{Q}_{\min}^2 calculated from the kinematics of the electron quark subsystem using the same values for the quark masses as in [3].

The missing information on the input distribution $D_{\gamma/P}$ is the most important source for the uncertainties of the predictions that we can give for the radiative cross section. They are especially important in the small- x large- y range. Calculations of the inclusive photon spectrum in $ep \rightarrow \gamma X$ [19] have shown that using either realistic structure functions in the low \hat{Q}^2 region or parton distribution functions designed to describe the large \hat{Q}^2 data can lead to considerable differences. It is important to realize that the Compton contribution appears as events which have a clean experimental signature: they contain an electron and a photon both with large transverse momentum balancing each other and some hadronic activity close to the proton beam. These events can consequently be identified experimentally, and HERA will be able to obtain information exactly on that part of the radiative corrections which makes their prediction at present uncertain [20].

4 Results for the differential cross section $d^2\sigma/dx dy$

In order to compare results of HERACLES with former calculations and to check the algorithm we have written a version of the Monte Carlo where x and y can be fixed as input and the integration is performed only over the phase space of the additional photon. We performed this investigation using the now obsolete values for the boson masses $M_W=82$ GeV and $M_Z=93$ GeV. The quark masses are $m_f=41$ MeV* and the parton distributions of [21] have been used. The results for

$$\delta_{\text{lep}}(x, y) = \frac{d^2\sigma/dx dy|^{(\alpha)}}{d^2\sigma/dx dy|_{\text{Born}}} - 1, \quad (10)$$

where $d^2\sigma/dx dy|^{(\alpha)}$ includes only leptonic QED corrections are shown in Fig. 3.

We find very good agreement at the 1% level except for very large y and small x where the corrections become large of the order of 100% and at large x and small y where the Monte Carlo results agree slightly better with [1] than with [3] (the difference of these two calculations are of the order of 3% at $x=0.99$ and $y \leq 0.4$).

As a check of the reliability of the program we have investigated the dependence of the results on the infrared cutoff k_0 . Because the allowed range for the photon energy is varying strongly with x and y , we did not fix k_0 , but instead the ratio

$$\varepsilon = \frac{k_0}{E_{\gamma, \min}(x, y; 1)},$$

with

$$E_{\gamma, \min}(x, y; 1) = \frac{2E_e E_p y(1-x)}{yE_e + (1-xy)E_p + \sqrt{4xy(1-y)E_e E_p + [yE_e - (1-xy)E_p]^2}},$$

where $E_{\gamma, \min}$ is the maximal photon energy minimized with respect to the emission angle in the HERA-laboratory reference frame. Figure 4 shows the ε dependence of the leptonic corrections for the selected point $x=0.1$, $y=0.9$. In this figure we also show the separate contributions of the soft and virtual corrections and the sum of the radiative channels (hard bremsstrahlung). These separate parts vary strongly with ε , whereas the sum of both remains sufficiently independent of ε as it should be. It varies by at most 0.1% in the range $10^{-4} \leq \varepsilon \leq 10^{-1}$. This is of the order of the statistical error of the Monte Carlo integration. In practice we have chosen $\varepsilon = 2 \times 10^{-2}$. This corresponds to a value of k_0 between 1 MeV for $x=0.9$, $y=0.02$ and 600 MeV for $x=0.1$, $y=0.98$. This choice is dictated by the requirements that i) ε should be chosen as small as possible, in order that the soft photon approximation used in the calculation of the non-radiative channel does not introduce large errors, but ii) ε should not be so small that the cross

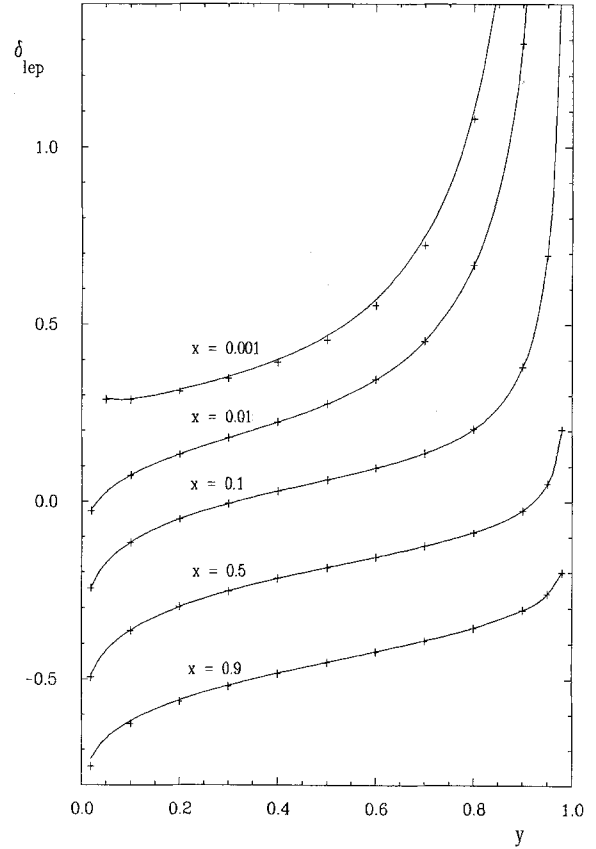


Fig. 3. Leptonic corrections for $e^- p \rightarrow e^- X$ at $S=10^5$ GeV, $x=0.9$, $x=0.5$, $x=0.1$, $x=0.01$ and $x=0.001$. The full lines are results of [3], the crosses are from HERACLES

section for the non-radiative channel becomes negative, since this would prevent from using a Monte Carlo approach where cross sections are interpreted as probabilities. This can happen for large x and small y . With $\varepsilon = 2 \times 10^{-2}$ one can still reach values for x up to 0.8 with $y \geq 0.15$ or $x \leq 0.6$ for $y \geq 0.02$. Once exponentiation of soft photonic corrections is included in the program one could choose a smaller value for ε and reach larger x and smaller y . The results shown in Fig. 4 are typical also for other values of x and y if ε is changed in the same range which, however, corresponds to a different range of k_0 .

From these investigations we roughly estimate the range of reliability of HERACLES as

$$10^{-3} \leq x \leq 0.9, \quad 0.02 \leq y \leq 0.95. \quad (11)$$

In this range the results of HERACLES and of the calculations of references [1] and [3] differ by not more than 3%. In the smaller region $2 \times 10^{-3} \leq x \leq 0.9$ and $0.1 \leq y \leq 0.9$ the differences are even below 1%. Both HERACLES and the program used in [3] have not been optimized in the very small x and very large y region and it is still possible to improve the reliability of the programs there.

* With the choice $m_f=41$ MeV for the light quark masses, the perturbative calculation of the fermionic contributions to the vacuum polarization agrees with the result derived from experimental data on $e^+ e^- \rightarrow \text{had}$ [22]

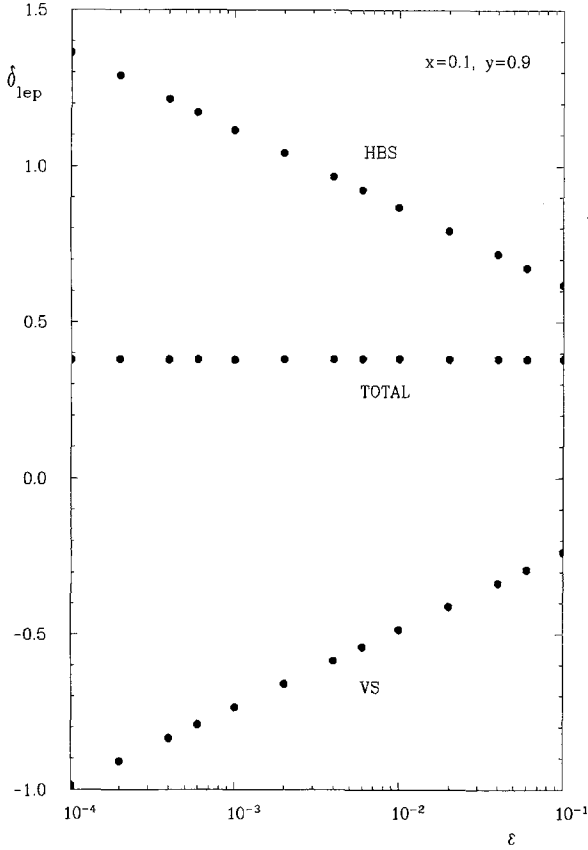


Fig. 4. Dependence of the leptonic corrections on the infrared cutoff ε for $x=0.1, y=0.9$. The upper points labelled HBS are the results of the hard bremsstrahlung contributions (initial and final state radiation and Compton part), the lower points (VS) describe virtual and soft photon corrections. TOTAL is the sum of both

5 Results for event distributions

In this section we discuss the results of a run of HERACLES which produced a sample of 6000 radiative events in a narrow bin $0.075 \leq x \leq 0.125$ and $0.8 \leq y \leq 0.9$. In order not to produce a large number of uninteresting soft photon events, we have restricted the kinematical range to $E_\gamma \geq 0.5$ GeV. Here we have used $M_Z = 91.1$ GeV, the coupling constants have been calculated from the μ decay using the radiatively corrected $M_W - M_Z$ relation leading to $\sin^2 \theta_W = 0.234$ (for $m_{top} = 80$ GeV, $M_{Higgs} = 100$ GeV), the quark masses were $m_f = 41$ MeV, and the parton distribution parametrizations have been taken from [23] (set B). The beam energies are $E_e = 30$ GeV and $E_p = 820$ GeV, i.e. $S = 98400$ GeV².

The total radiative cross section in the considered range $0.075 \leq x \leq 0.125$, $0.8 \leq y \leq 0.9$ and $E_\gamma \geq 0.5$ GeV is 0.49 pb corresponding to about 100 events in a year at HERA (with 200 pb^{-1} integrated luminosity expected). The total $\mathcal{O}(\alpha)$ corrected cross section including radiative and non-radiative contributions in the same bin is 0.88 pb. With the lowest order cross section being 0.62 pb this corresponds to a correction of about 43%.

Figure 5a shows the distribution of these events versus the emission angle of the photon θ_γ which is mea-

sured with respect to the electron direction. In the figure one recognizes the peak of the initial state radiation at $\theta_\gamma = 0$. Its width can be calculated approximately from the differential cross section if one takes into account only the essential factor $1/k p_e = 1/E_\gamma (E_e - |\mathbf{p}_e| \cos \theta_\gamma)$: the median is

$$\theta_\gamma^m = \sqrt{2 \frac{m_e}{E_e}} \simeq 6 \text{ mrad} \quad (12)$$

The final state radiation is peaked in the direction of the outgoing electron which is given by:

$$\cos \theta'_e = \frac{(1-y) E_e - x y E_p}{(1-y) E_e + x y E_p} \quad (13)$$

For $0.075 \leq x \leq 0.125$ and $0.8 \leq y \leq 0.9$ the electron scattering angle varies from 142° to 160° . Consequently also the peak from final state emission is smeared out over this range. If x and y would have been fixed one would have found a narrow peak with a width $\simeq \sqrt{2 m_e / E'_e}$. Finally the Compton peak $\hat{Q}^2 \rightarrow 0$ is also visible as a broad bump in the range of θ_γ from 51° to 85° (see (5)). This peak is more pronounced for smaller values of x and large values of y but disappears at large x and small y .

Figure 5b shows the same sample of events distributed over the energy of the photon E_γ . The Compton part that we have just discussed is also clearly visible in this figure at $E_\gamma \simeq 35$ GeV. The soft photon peak at $E_\gamma = 0$ is cut at the lower end of the spectrum by the condition $E_\gamma \geq 0.5$ GeV. In addition to these peaks one finds also an accumulation of events at an energy $E_\gamma \simeq 23$ GeV. This enhancement of the cross section at a rather large photon energy is due to the combined effect of the factors $1/z_1$ and $1/\hat{Q}^2$ in the differential cross section. The first factor is big for initial state collinear radiation. In the case where $\theta_\gamma = 0$ one finds

$$\hat{Q}^2 = 2(E_e - E_\gamma) E'_e (1 - \cos \theta'_e). \quad (14)$$

Thus the second factor is largest if E_γ is as close as possible to the energy of the initial electron. For emission of photons parallel to the incoming electron the maximally allowed photon energy is

$$E_\gamma^{\max}(\theta_\gamma = 0) = y \frac{1-x}{1-xy} E_e \quad (15)$$

which describes the position of the peak in the photon energy distribution below $E_e = 30$ GeV.

We show also in Figs. 5c and 5d the distribution of the events versus the energy of the scattered quark E'_q and its scattering angle θ'_q (again defined with respect to the electron direction). It is expected that these distributions determine also the distributions of the energy and angle of the current jet, although there will be a small systematic shift from the quark scattering angle to the current jet angle due to the string effect and hadronization effects will lead to some smearing. The E'_q distribution in Fig. 5c is peaked in the range from 33 GeV to 44 GeV according to (5). The events found

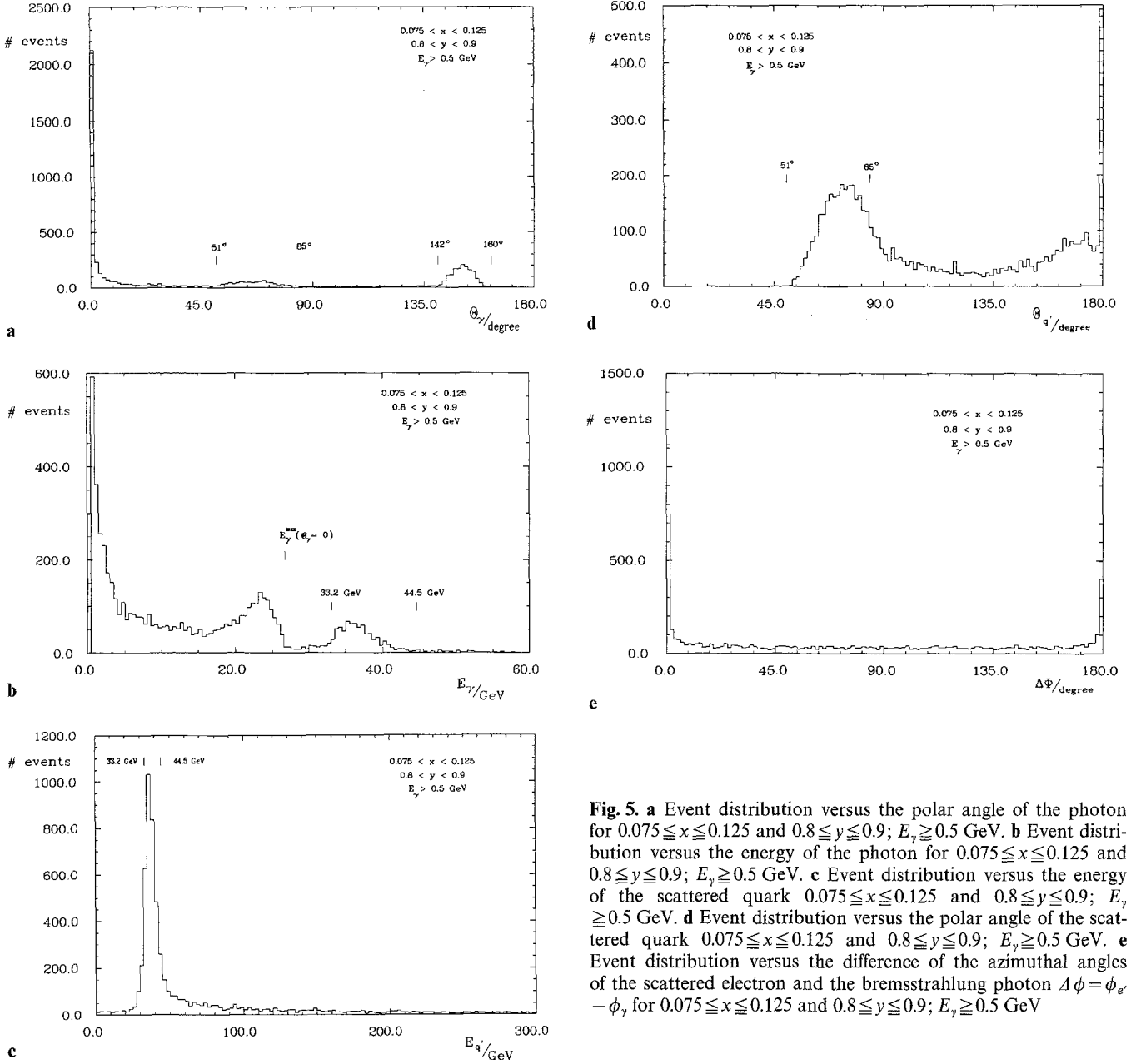


Fig. 5. **a** Event distribution versus the polar angle of the photon for $0.075 \leq x \leq 0.125$ and $0.8 \leq y \leq 0.9$; $E_\gamma \geq 0.5$ GeV. **b** Event distribution versus the energy of the photon for $0.075 \leq x \leq 0.125$ and $0.8 \leq y \leq 0.9$; $E_\gamma \geq 0.5$ GeV. **c** Event distribution versus the energy of the scattered quark $0.075 \leq x \leq 0.125$ and $0.8 \leq y \leq 0.9$; $E_\gamma \geq 0.5$ GeV. **d** Event distribution versus the polar angle of the scattered quark $0.075 \leq x \leq 0.125$ and $0.8 \leq y \leq 0.9$; $E_\gamma \geq 0.5$ GeV. **e** Event distribution versus the difference of the azimuthal angles of the scattered electron and the bremsstrahlung photon $\Delta\phi = \phi_e - \phi_\gamma$ for $0.075 \leq x \leq 0.125$ and $0.8 \leq y \leq 0.9$; $E_\gamma \geq 0.5$ GeV

here are events containing a soft photon. In addition to them one recognizes a rather long tail of events reaching to large quark energies which are due to hard photon bremsstrahlung. This is a paradoxical situation: the emission of energy by a photon can lead to the appearance of a more energetic final state quark. This can be explained from the fact that the total energy entering into the hard scattering is not fixed but the proton must be viewed as a wide-band beam of incoming quarks with energies ranging up to the maximum of $E_p = 820$ GeV. In the non-radiative case the energy of the initial quark can be reconstructed from the momentum of the scattered electron and the energy of the final quark is then also determined by (5). However, photon emission allows for scattering with larger *cms*-energy and therefore higher energetic outgoing quarks are also possible.

In the distribution with respect to the angle of the scattered quark (Fig. 5d) one can again find several peaks. The events with a soft photon are located in the range from 51° to 85° . The accumulation of events at $\theta_q = 180^\circ$ is resulting from the Compton peak. Slightly below 180° at $\theta_q \simeq 170^\circ$ one recognizes the peak of events which contain a photon collinear with the incoming electron and small \hat{Q}^2 (large energy $E_\gamma \simeq 23$ GeV).

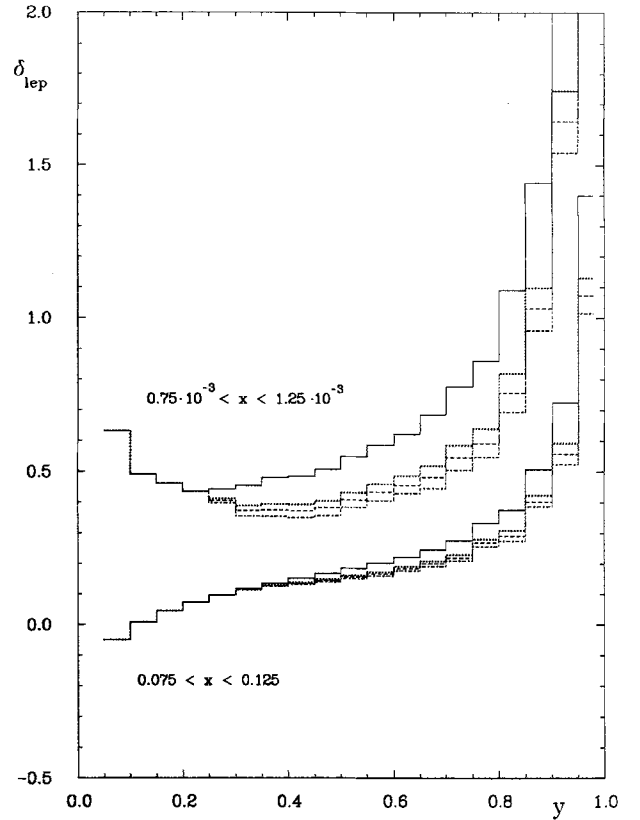
Finally, Fig. 5e shows the event distribution with respect to the difference of the azimuthal angles of the scattered electron and the bremsstrahlung photon. Superimposed over a uniform distribution coming from initial state radiation, one finds a peak at $\Delta\phi = 0^\circ$ resulting from final state radiation and again the Compton contribution with low- \hat{Q}^2 events is outstanding as a smaller peak at $\Delta\phi = 180^\circ$.

6 Cuts

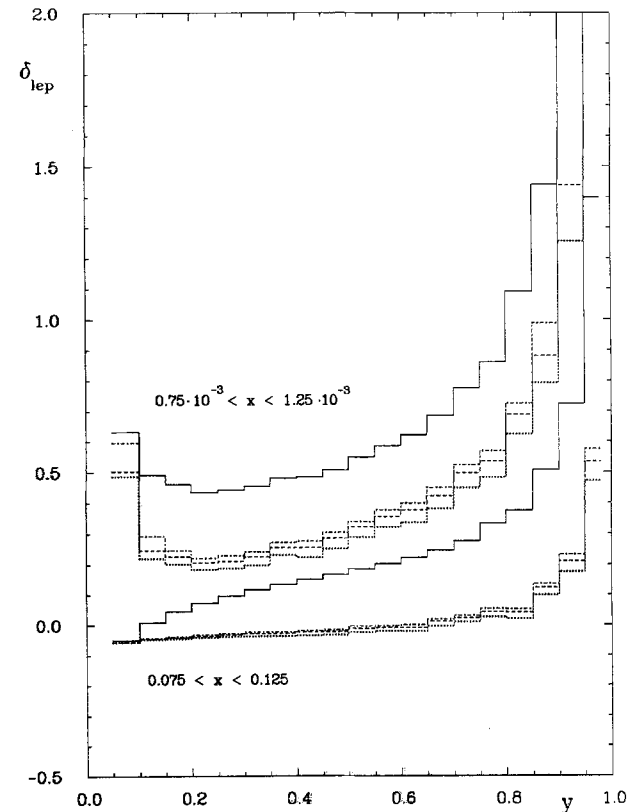
The results of the preceding section have shown that a considerable number of events in ep scattering have a photon with large energy and large emission angle. These events are potentially visible in the detector, and being recognized as radiative events they could be discarded from the sample of events which is used to perform a physics analysis. In this section we want to study the possibility of reducing radiative corrections by applying cuts on the event samples based on the observability of photons.

In order to be visible, a photon has to have enough energy and its direction has to be such that it hits an active element of the detector. In addition there is the possibility to observe a photon indirectly because the emission of momentum by a photon disturbs the relation of energies and scattering angles of the electron and the hadron jet as it would be expected for events without (or only soft) photons.

The aim of the following discussion is to present first ideas of how radiative events could eventually be identified and thereby to show up directions for further studies. A complete investigation will have to start with a Monte Carlo which also simulates hadronization effects in order to include photons occurring during the evolution of the quark cascade, photons from hadron bremsstrahlung and hadron decays, as well as broadening of the current jet and systematic shifts of the angle and energy of the original parton from which the current jet is emerging. Eventually, it will also be necessary to perform a detector simulation taking into account the non-perfect coverage of the detector, smearing and acceptance, misidentification of photons etc. This was not done here and therefore the results shown below should be understood as belong-

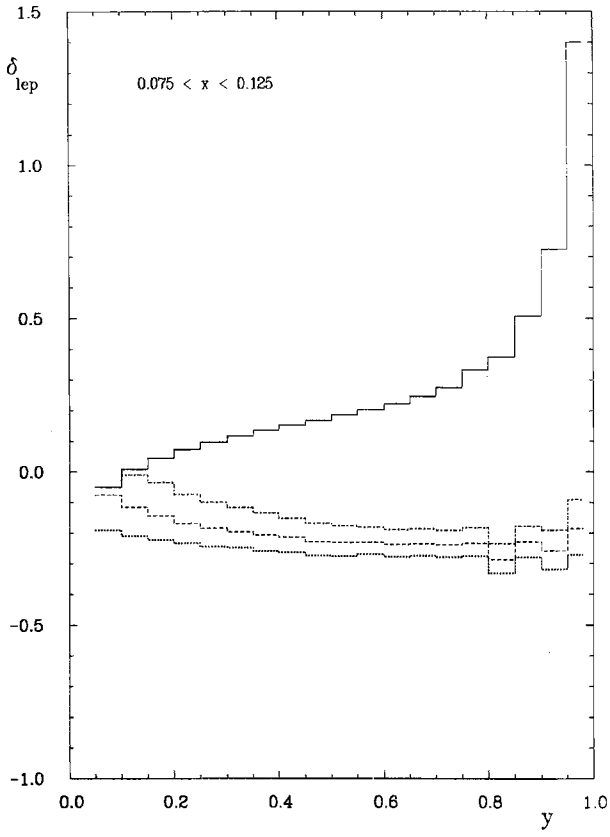


a

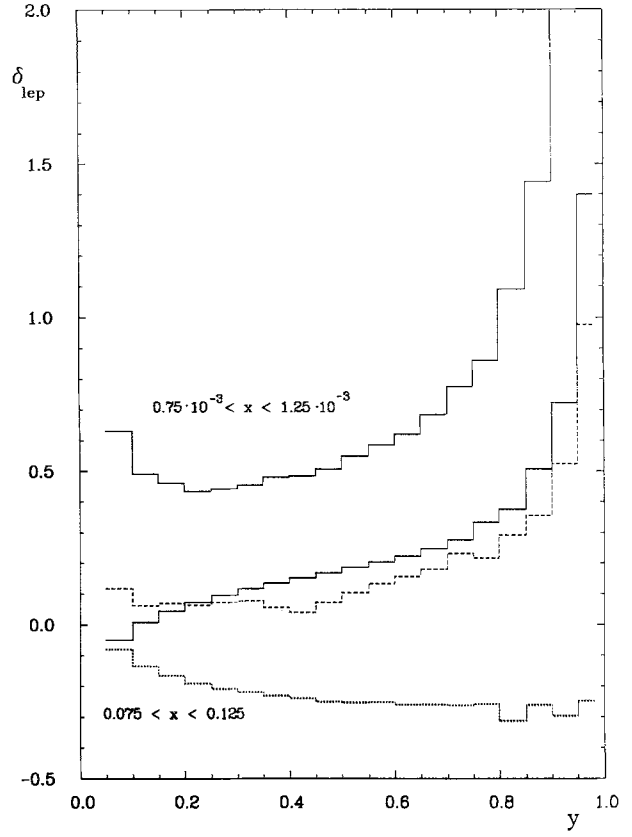


b

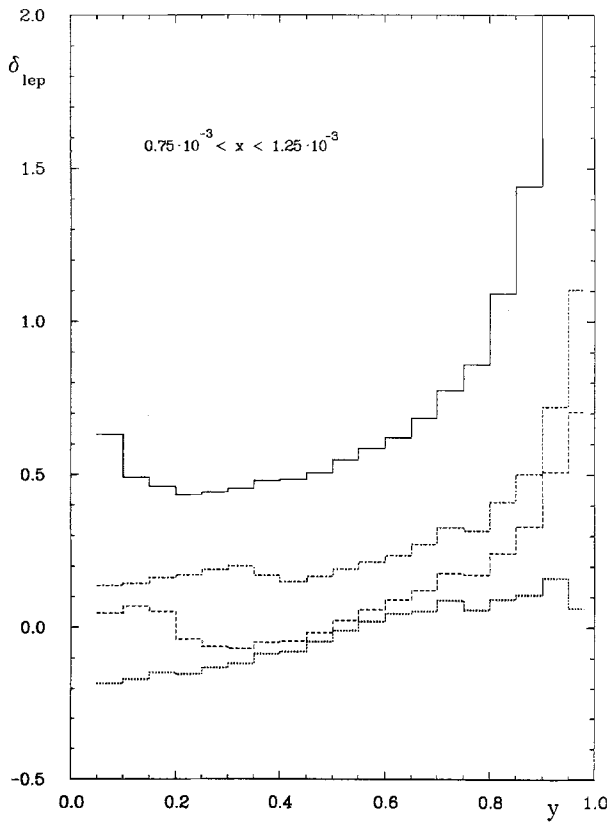
Fig. 6. **a** Influence of a forward detector cut on the radiative corrections in the range $0.075 \leq x \leq 0.125$ and $0.75 \times 10^{-3} \leq x \leq 1.25 \times 10^{-3}$. $\theta_\gamma \leq 0.5$ mrad (dotted line), $\theta_\gamma \leq 1.0$ mrad (dashed line), $\theta_\gamma \leq 2.0$ mrad (dashed-dotted line), always with $E_\gamma \geq 8$ GeV. **b** Influence of an angular cut on the radiative corrections in the range $0.075 \leq x \leq 0.125$ and $0.75 \times 10^{-3} \leq x \leq 1.25 \times 10^{-3}$. $2^\circ \leq \theta_\gamma \leq 178^\circ$ (dotted line), $4^\circ \leq \theta_\gamma \leq 176^\circ$ (dashed line), $6^\circ \leq \theta_\gamma \leq 174^\circ$ (dashed-dotted line), $E_\gamma \geq 2$ GeV. **c** Influence of the cut C_3 using a jet measurement in the range $0.075 \leq x \leq 0.125$. $\theta_{D,\min} = 10^\circ$ (dotted line), $\theta_{D,\min} = 20^\circ$ (dashed line), and $\theta_{D,\min} = 30^\circ$ (dashed-dotted line). **d** Influence of the cut C_3 using a jet measurement in the range $0.75 \times 10^{-3} \leq x \leq 1.25 \times 10^{-3}$. $\theta_{D,\min} = 20^\circ$. $E_{q',\min} = 0$ (dotted line), $E_{q',\min} = 5$ GeV (dashed line), and $E_{q',\min} = 10$ GeV (dashed-dotted). **e** Influence of a combined cut on the radiative corrections in the range $0.75 \times 10^{-3} \leq x \leq 1.25 \times 10^{-3}$ (dashed line) and $0.075 \leq x \leq 0.125$ (dotted line). $4^\circ \leq \theta_\gamma \leq 176^\circ$ and $E_\gamma \geq 2$ GeV and $\theta_{D,\min} = 20^\circ$, $E_{q',\min} = 10$ GeV. The full lines show the corresponding total corrections. **f** Influence of a cut on the dependence of radiative corrections on parton parametrizations in the range $0.75 \times 10^{-3} \leq x \leq 1.25 \times 10^{-3}$. The upper curves show the total corrections for HMRS (set E) [23] and DO [21]. The effect of the cut is demonstrated by the lower curves: HMRS (set E) (dashed) and DO (dotted). $4^\circ \leq \theta_\gamma \leq 176^\circ$ and $E_\gamma \geq 2$ GeV and $\theta_{D,\min} = 20^\circ$, $E_{q',\min} = 10$ GeV



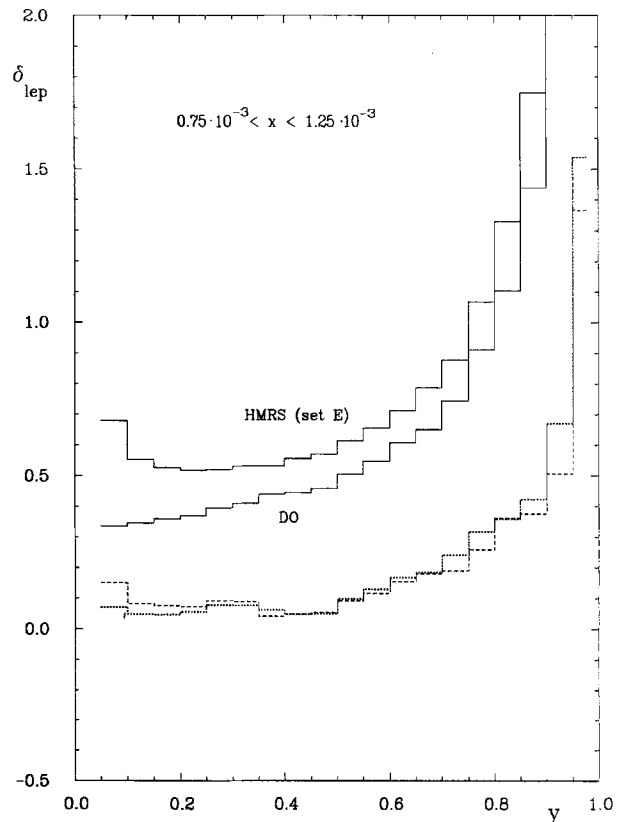
c



e



d



f

Fig. 6c-f

ing to a rather optimistic scenario and the reduction of radiative corrections that we found are certainly those which are maximally reachable.

To start with we discuss separately several features of a simple idealization of the H1 or ZEUS detectors. In each case we have calculated the cross sections and the resulting corrections* in bins with x ranging from 0.075 to 0.125 or from 0.75×10^{-3} to 1.25×10^{-3} and y in intervals of width $\Delta y = 0.05$ starting from $y = 0.05$ to $y = 0.95$ and one last interval of $0.95 \leq y \leq 0.98$. In each of these bins sampled events where analysed and rejected if they satisfied some simple criterion for observability. From the remaining number of events the reduced radiative corrections have been determined.

- First we assume that events with a photon emitted collinearly with the incoming electrons and thus hitting the luminosity monitor can be identified if the photon is not too soft. The actual acceptances in the ZEUS or H1 forward detectors are rather complicated functions of the emission angle [24]. We simplify the situation and define a first cut by

$$C_1: 0^\circ \leq \theta_\gamma \leq \theta_{FD} \quad \text{and} \quad E_\gamma \geq 8 \text{ GeV}. \quad (16)$$

In Fig. 6a we show the reduced corrections after subtracting those events that satisfy C_1 , i.e. which can be identified in this idealized forward detector for the values of $\theta_{FD} = 0.5, 1, \text{ and } 2$ mrad. The dependence on θ_{FD} is rather mild because we have used a large (but even optimistic) detection threshold for the photons of $E_\gamma^{\min} = 8$ GeV. It is seen that only at large values of y the cut C_1 can reduce the corrections by 10–30% at $x \simeq 0.1$ and by 50–80% at $x \simeq 10^{-3}$ depending on the value of θ_{FD} **.

- A major part of the photons will be emitted with a large angle and these photons are thus hitting the main detector. In order to study the possibility to reduce the radiative corrections with the help of the main detector we imposed the cut

$$C_2: \theta_{AC} \leq \theta_\gamma \leq \pi - \theta_{AC} \quad \text{and} \quad E_\gamma \geq 2 \text{ GeV}. \quad (17)$$

Figure 6b shows the results for the corrections after events covered by cut C_2 are rejected for $\theta_{AC} = 2^\circ, 4^\circ, \text{ and } 6^\circ$. The effect of this cut is huge. Almost over the whole range of y the corrections for $x \simeq 0.1$ are reduced down to 0% and for $x \simeq 10^{-3}$ they remain below 50% over a much larger range of y than without cut. The results do not depend very strongly on the value taken for the minimal photon energy.

- The events that lead to corrections increasing with increasing y are mainly events with a hard photon close to the direction of the initial electron which are not always covered by either cut C_1 or C_2 . These events have \hat{Q}^2 values much smaller than Q^2 . Consequently the scattered quark appears closer to the proton direction than

it is expected from the electron measurement of x and y . By checking the kinematical relation between the scattered electron and the current jet and rejecting all events that are not consistent with non-radiative kinematics one can gain a further reduction of the radiative corrections. In most cases it will not be possible to identify uniquely a current jet and to measure the energy or the angle of that jet. Rather one should think of comparing the results of the electron measurement of the scaling variables x_e, y_e using (1) with that obtained by using the Jaquet-Blondel method via the measurement of the total hadron flow. This method will give values x_h, y_h which will differ from x_e and y_e not only due to experimental uncertainties in the measurement of the hadronic final state, but the presence of an unobserved photon will lead to large differences of these two sets of variables. The present version of our Monte Carlo does not perform a hadronization of the scattered quark and the proton remnant. Therefore we are not able to perform a study of the effect of photon bremsstrahlung on the determination of x_h and y_h , but assume that the angle θ_D between the momentum of the actually emitted quark \mathbf{p}_q , and the direction of the jet $\mathbf{p}_{J,0}$ as it is calculated from the electronic measurement of x_e and y_e using non-radiative kinematics is a measure of $|x_e - x_h|$ and $|y_e - y_h|$. For $x \simeq 0.1$ we show in Fig. 6c the effect of rejecting events satisfying the cut

$$C_3: \theta_D = \angle(\mathbf{p}_q, \mathbf{p}_{J,0}) \geq \theta_{D,\min}. \quad (18)$$

For $\theta_{D,\min}$ we have chosen the values $10^\circ, 20^\circ, \text{ and } 30^\circ$ and for $0.075 \leq x \leq 0.125$ we find huge reductions down to values below 0% even at very large y . The results for the corrections after cut don't depend very strongly on the actual value of $\theta_{D,\min}$ which means that a good accuracy of the jet angle measurement is not essential. Note, that we did not use the energy of the scattered quark for the cross-checking of kinematics. An additional cut on $\Delta E_q = |E_q - E_q^0|$ could lead to a further reduction of the radiative corrections. The results obtained here with the help of a Monte Carlo treatment of the exact $\mathcal{O}(\alpha)$ leptonic corrections are in good agreement with a leading-log calculation [18].

As a prerequisite of the applicability of a cut on the jet angle, the jet has of course to come out with an energy big enough so that it can be identified as a jet. This is the case for larger values of x . Indeed, requiring a minimal jet energy of 20 GeV would not change the results shown in Fig. 6c essentially. Only in the last bin $0.95 \leq y \leq 0.98$ the corrections would be bigger by about 5% than without this additional condition.

For smaller values of x however, the jet energies are generally smaller and the additional condition $E_q \geq E_{q,\min}$ prevents from reaching similarly big reductions. In Fig. 6d we show results for $0.75 \times 10^{-3} \leq x \leq 1.25 \times 10^{-3}$ for the effect of the cut C_3 with $\theta_{D,\min} = 20^\circ$ for several values for $E_{q,\min}$. In spite of the more difficult situation, reductions of the order of 50% can be reached. For $E_{q,\min} = 10$ GeV the corrections after cut stay below 50% up to values of $y \simeq 0.9$. The reduction of radiative corrections shown in Fig. 6d are perhaps not those

* The corrections discussed in this section contain also photon and Z boson self energies

** The possibility to handle QED bremsstrahlung effects at HERA by photon tagging with the help of the luminosity monitor was discussed also in [25]

which are maximally reachable because of the following reason: the events which have a small jet energy have at the same time a jet angle close to 90° . It might be possible that for these events a smaller value for the cut angle than $\theta_{D,\min}=20^\circ$ could be realized.

One could also ask whether at small x the jets are not too close to the electron beam hole which is the case for the non-radiative events above a certain limit of y . Too many particles belonging to the current jet can then be lost and a precise measurement of x_h and y_h is no more possible. However, it turned out that many events have a hard bremsstrahlung photon which turns the scattered quark back into the central region of the detector so that radiative events can be identified because they have a clearly visible jet although from the electron measurement there was none expected. The cut C_3 always implies that the current jet has to be at least 10° away from the beam holes if the non-radiative jet was expected to be closer than 10° or vice versa. Only in that case where the current jet expected from the electron measurement should be close to the electron beam hole and the actual jet is also, one has to answer the question whether a deviation of x_h and y_h from x_e and y_e is due to a loss of particles belonging to the current jet or whether it could have been also a missed bremsstrahlung photon. In practice, it will not be possible to give an answer to this question for single events, but we believe that future Monte Carlo studies will show how to use the characteristics of the hadron flow on a statistical basis in order to keep corrections due to events of this type small.

Bearing these caveats in mind, the possibility of comparing electronic and hadronic measurements of the scaling variables is nevertheless promising to provide a significant reduction of radiative corrections.

● All the cuts investigated above addressed different detector features or methods of photon identification. Yet for the reduction of radiative corrections the mere appearance of a photon is of concern, no matter in which way it is tagged. We therefore have also considered a combination of the mentioned cuts. From our sampled events we rejected those which satisfy one of the conditions of the following combined cut

$$C_4 \text{ (i) } \theta_{AC} \leq \theta_\gamma \leq \pi - \theta_{AC} \quad \text{and} \quad E_\gamma \geq 2 \text{ GeV} \\ \text{(ii) } \theta_D \geq \theta_{D,\min} \quad \text{and} \quad E_{q'} \geq E_{q',\min}. \quad (19)$$

As parameters we chose $\theta_{AC}=4^\circ$, $\theta_{D,\min}=20^\circ$ and $E_{q',\min}=10 \text{ GeV}$. We have not included the cut C_1 here because condition ii) of C_4 already rejects events with photons of large energy emitted in the direction of the initial electron. The reduced radiative corrections are shown in Fig. 6e for two different x -bins. Whereas for the bins with $x \approx 0.1$ the radiative corrections after cut stay slightly below 0% and are very weakly dependent on y , for the smaller $x \approx 10^{-3}$ the corrections still become large at large y but they reach 50% only for $y \geq 0.95$. This is a considerable improvement as compared to the corrections without any cut.

Parton distribution functions as a basic ingredient for the theoretical study of deep inelastic processes influence

considerably the accuracy to which radiative corrections can be predicted. Fig. 6f shows results of a comparison of two different input distributions. We have applied the last cut C_4 on two samples of events in the same x -region $0.75 \times 10^{-3} \leq x \leq 1.25 \times 10^{-3}$. For the first sample the parton parametrization of [23] (set E) is used, while for the second we took the parton distributions of [21] as input. The total corrections are clearly distinct. The results for the corrections after cutting out observable radiative events, however, are very similar to each other. This fact should simplify the physics analysis of experimental data considerably. In turn it also means that the observable radiative events themselves have a potential for obtaining information on the structure functions.

7 Conclusion

In this article we have given a description of the Monte Carlo HERACLES for deep inelastic ep scattering including radiative effects. This program is able to describe the differential cross section for scattering of polarized electrons and positrons with an accuracy of a few percent. The spectrum of bremsstrahlung photons in the vicinity of the directions of the initial and final lepton is recovered correctly, its description being based on the exact $\mathcal{O}(\alpha)$ expression for the leptonic bremsstrahlung cross section.

HERACLES was used to study the features of deep inelastic ep events with a bremsstrahlung photon in the final state. It has been shown that a major contribution to the radiative corrections are due to hard photon emission. Photons are radiated mainly with large angle or into the electron direction changing thereby the kinematical relation between the scattered electron and the current jet. Consequently a large number of radiative events can be identified and radiative corrections can be considerably reduced.

The cuts that we have discussed should help to find a clean sample of events which can be used to perform a simplified physics analysis without too much complications due to radiative corrections. But the events selected by the above cuts are also interesting by themselves. They should be used to study the dynamics of deep inelastic scattering and it could be possible that their analysis will also contribute to a determination of structure functions. This analysis will be rather straightforward for two classes of events: i) events with an observed photon will allow a reconstruction of the actual momentum transfer $\hat{Q}^2 = (p_e - p'_e - k)^2$ and the correct partonic $\hat{x} = \hat{Q}^2 / 2P(p_e - p'_e - k)$ and ii) for events with a photon collinear to the final electron the calorimetric measurement automatically provides a determination of the summed momenta $p_e + k$ and thus also determines \hat{Q}^2 and \hat{x} . For these event samples no unfolding will be necessary. Whether those radiative events which can be identified only indirectly by the comparison of electronic and hadronic measurements of x and y can also be used to get information on the structure functions is more questionable and would need further investigations.

Appendix

In this appendix we present the complete set of formulas and definitions needed for the calculation of the cross sections for $ep \rightarrow eX$ and $ep \rightarrow e\gamma X$. In the following we neglect fermion masses and assume $m_f^2 \ll S, Q^2$.

Lowest order cross section

For scattering of electrons or positrons with degree of longitudinal polarization P_L the cross section reads:

$$\frac{d^2\sigma}{dx dy} \Big|_{e^\pm}^{\text{Born}} = \frac{2\pi\alpha^2}{xyQ^2} \sum_{i,j} \chi_i \chi_j \left\{ \sum_f A_f^{ij} [1 + (1-y)^2] x(q_f(x) + \bar{q}_f(x)) \mp \sum_f B_f^{ij} [1 - (1-y)^2] x(q_f(x) - \bar{q}_f(x)) \right\}, \quad (20)$$

where $\chi_\gamma=1$ and the γZ interference and the pure Z exchange contain the reduced Z propagator

$$\chi_Z(Q^2) = \frac{Q^2}{Q^2 + M_Z^2}. \quad (21)$$

The coupling constants enter in the combinations

$$\begin{aligned} A_f^{ij} &= (\lambda_V^{ij} - P_L \lambda_A^{ij}) \lambda_V^{fij}, \\ B_f^{ij} &= (\lambda_A^{ij} - P_L \lambda_V^{ij}) \lambda_A^{fij}, \end{aligned} \quad (22)$$

with

$$\begin{aligned} \lambda_V^{ij} &= v_f^i v_f^j + a_f^i a_f^j, \\ \lambda_A^{ij} &= v_f^i a_f^j + a_f^i v_f^j, \end{aligned} \quad (23)$$

v_f^i and a_f^i are the vector and axial vector coupling constants of the vector bosons $i=\gamma, Z$ to the fermions given by their charge Q_f and isospin I_3^f :

$$v_f^\gamma = Q_f, \quad a_f^\gamma = 0, \quad (24)$$

$$v_f^Z = \frac{I_3^f - 2s_W^2 Q_f}{2s_W c_W}, \quad a_f^Z = \frac{I_3^f}{2s_W c_W}. \quad (25)$$

The weak mixing angle is determined by the gauge boson masses:

$$c_W = \cos \theta_W = \frac{M_W}{M_Z}, \quad s_W^2 = 1 - c_W^2. \quad (26)$$

Bremsstrahlung cross section ($ep \rightarrow e\gamma X$)

For the radiative process we use in addition to x, y , and Q^2 the following kinematical variables:

$$\begin{aligned} s &= (p_e + p_q)^2, & t &= (p_e - p'_e)^2, & u &= (p_e - p'_q)^2, \\ s' &= (p'_e + p_q)^2, & t' &= (p_q - p'_q)^2, & u' &= (p'_e - p_q)^2, \\ Q^2 &= -t, \\ \hat{Q}^2 &= -t', \end{aligned} \quad (27)$$

and

$$z_1 = 2(k \cdot p_e), \quad z_2 = 2(k \cdot p'_e). \quad (28)$$

The variable \hat{x} defines the center-of-mass energy of the electron quark subsystem by $s = \hat{x}S$. Then \hat{x} is the argument of the parton distribution functions and the cross section for electron proton scattering reads

$$\sigma = \sum_f \int d\hat{x} \frac{2\pi^2}{\hat{x}S} \int d^{(3)}PS q_f(\hat{x}, \mu^2) |\mathcal{M}_f|^2 \quad (29)$$

The factorization scale μ^2 in the parton distributions has been chosen to be \hat{Q}^2 as is suggested from a model-independent calculation in the one-photon-exchange approximation. The spin averaged modulus squared of the matrix element describing leptonic radiation is

$$\begin{aligned} |\mathcal{M}_f|^2 &= \frac{\alpha^3}{32\pi^4} \sum_{i,j=\gamma,Z} \frac{1}{(t' - M_i^2)(t' - M_j^2)} \\ &\cdot \left\{ \frac{-t'}{k p_e k p'_e} [A_f^{ij}(s^2 + s'^2 + u^2 + u'^2) \right. \\ &+ B_f^{ij}(s^2 + s'^2 - u^2 - u'^2)] \\ &- \frac{m_e^2}{(k p_e)^2} [2A_f^{ij}(s'^2 + u'^2) + 2B_f^{ij}(s'^2 - u'^2)] \\ &\left. - \frac{m_e^2}{(k p'_e)^2} [2A_f^{ij}(s^2 + u^2) + 2B_f^{ij}(s^2 - u^2)] \right\}. \end{aligned} \quad (30)$$

The 3-particle phase space

$$\int d^{(3)}PS = \int \frac{d^3 p'_e}{2E'_e} \frac{d^3 p'_q}{2E'_q} \frac{d^3 k}{2E_\gamma} \delta^4(p_e + p_q - p'_e - p'_q - k) \quad (31)$$

can most conveniently be parametrized in the reference frame where $\mathbf{k} + \mathbf{p}'_q = 0$ (i.e. the center-of-mass reference frame of the outgoing quark and the emitted photon).

$$\begin{aligned} \int d^{(3)}PS &= \frac{\pi y S}{2} \frac{\sqrt{\lambda(s_2, m_q, 0)}}{8s_2} dx dy d \cos \theta_\gamma^* d \phi_\gamma^* \\ &= \frac{\pi y S}{2} \frac{E_\gamma^*}{4(E_e^* + E_q^* - E_e'^*)} dx dy d \cos \theta_\gamma^* d \phi_\gamma^* \end{aligned} \quad (32)$$

where $s_2 = (k + p'_q)^2$ and $\lambda(x, y, z) = x^2 + y^2 + z^2 - 2xy - 2xz - 2yz$. We used starred symbols to denote energies and angles in the cms -system. In this reference frame the energies of the scattering particles are expressed as functions of x, y , and \hat{x} :

$$\begin{aligned} E_q^* &= \frac{\hat{x}yS - 2m_e^2}{2E_{\text{tot}}} \\ E_e^* &= \frac{(\hat{x} - xy)S - m_e^2 - m_q^2}{2E_{\text{tot}}}, \\ E_e'^* &= \frac{(xy + \hat{x}(1-y))S + m_e^2 + m_q^2}{2E_{\text{tot}}}, \\ E_\gamma^* &= \frac{(\hat{x} - x)yS - M^2}{2E_{\text{tot}}}, \\ E_q^* &= E_e^* + E_q^* - E_e'^* - E_\gamma^* = \sqrt{E_\gamma^{*2} + m_q^2}, \\ E_{\text{tot}} &= E_e^* + E_q^* - E_e'^* = \sqrt{(\hat{x} - x)yS - 2m_e^2 - m_q^2}, \end{aligned} \quad (33)$$

where $M^2 = 2(m_e^2 + m_q^2)$ is the sum of the squares of all involved fermions.

In addition to this form we need also a parametrization of the phase space in terms of the invariants t' , z_1 , and z_2 . This has always the form

$$\int d^{(3)}\text{PS} = \frac{\pi y S}{2} \frac{1}{8\sqrt{-\Delta_4(p_e, p'_e, p_q, k)}} dx dy d\zeta_1 d\zeta_2 \quad (34)$$

where ζ_1, ζ_2 is one of the invariants $2kp_e, 2kp'_e$, or $t' = t - 2kp_e + 2kp'_e$. The Gram determinant Δ_4 has to be expressed accordingly with the help of the variables ζ_1 and ζ_2 .

Phase space limits

The phase space limits follow essentially from the condition $\Delta_4 \leq 0$, but there are additional non-trivial restrictions from the condition $E_\gamma \geq k_0$ which restricts the energy of the emitted photon in the HERA laboratory reference frame. This condition restricts not only the range of integration for \hat{x} but also for the angles of the photon in the cms -system. The minimum of \hat{x} is derived from

$$E_{\gamma, \max}(x, y; \hat{x}_{\min}) = k_0 \quad (35)$$

where $E_{\gamma, \max}(x, y; \hat{x})$ is the maximum of the photon energy with respect to the emission angle in the HERA laboratory system for fixed \hat{x} . It is given by

$$E_{\gamma, \max}(x, y; \hat{x}) = \frac{s+t+u-M^2}{2(s+t+u-M^2+m_f^2)} \cdot \{E_e + E_q - E'_e + \sqrt{(|\mathbf{p}_e| - |\mathbf{p}_q| - |\mathbf{p}'_e| \cos \theta'_e)^2 + |\mathbf{p}'_e|^2 \sin^2 \theta'_e}\} \quad (36)$$

where all energies and momenta and the electron scattering angle θ'_e are taken in the HERA reference frame. The solution of (35) for $k_0 = 0$ is $\hat{x}_{\min}(0) = x + M^2/yS$. For small k_0/E_e it is

$$\hat{x}_{\min} = x + \frac{M^2}{yS} + \frac{m_q^2}{yS} \frac{k_0}{yE_e + x(1-y)E_p}. \quad (37)$$

$$z_1^\pm = \frac{-t' [s(s+u) + t(s-u)] \pm \sqrt{-2tt'u(s+u)[t+2s+2st'(s+t+u)]}}{(s+u)^2} \quad (44)$$

Note that for fixed $\hat{x} > x + M^2/yS$ the emission of zero-energy photons is kinematically not allowed. Only for elastic scattering without emission of energy by an additional photon the Bjorken identification $\hat{x} = x$ is derived (up to terms of order $\mathcal{O}(m_q^2)$).

The conditions for the angular integration are determined by

$$E_\gamma(x, y, \hat{x}, \theta_\gamma, \phi_\gamma) \geq k_0 \quad (38)$$

and from them in turn one can calculate the limits for t', z_1, z_2 . Because we use different phase space parametrizations in the various channels we have also different sets of phase space limits in each channel:

● initial state radiation: The variables are x, y, \hat{x}, z_1 and t' in this order. The range of x and y is given as input by the user to the program. After having chosen values for x and y , \hat{x}_{\min} can be calculated from (35) and a choice for \hat{x} be made in the range $\hat{x}_{\min} \leq \hat{x} \leq 1$. This then fixes the center-of-mass energies (33). Equation (38) determines the range for the angular integration. For the initial state radiation the polar axis is chosen parallel to the incoming electron momentum and the limits for the polar angle $\theta_\gamma^{*\pm}$ lead to limits for z_1 :

$$z_1^\pm = 2E_\gamma^* (E_e^* - |\mathbf{p}_e^*| \cos \theta_\gamma^{*\pm}) \quad (39)$$

Finally, from $\Delta_4 \leq 0$ one can derive the limits for t' . Here we give only the approximate result obtained after neglecting the fermion masses:

$$t'_{(k_p)}^\pm = \frac{-z_1 [s(s+u) + t(s-u)] \pm 2\sqrt{z_1 s t u (s+t+u)(s+t-z_1)}}{(s+t)^2} \quad (40)$$

which is expressed as a function of z_1 besides x, y, \hat{x} .

● final state radiation: Here the variables are x, y, \hat{x}, z_2 , and t' . In this case the polar axis is chosen parallel to the outgoing electron momentum and (38) determines via the limits for the polar angle of the photon momentum $\theta_\gamma'^{* \pm}$

$$z_2^\pm = 2E_\gamma^* (E_e^* - |\mathbf{p}_e^*| \cos \theta_\gamma'^{* \pm}) \quad (41)$$

and from $\Delta_4 \leq 0$ (again for $m_f = 0$):

$$t'_{(k_p)}^\pm = \frac{-z_2 [s(t-u) - u(t+u)] \pm 2\sqrt{-z_2 s t u (s+t+u)(t+u+z_2)}}{(t+u)^2} \quad (42)$$

which is now a function of z_2 besides x, y, \hat{x} .

● Compton part: One proceeds in a similar way but the sequence of variables chosen in this case is x, y, \hat{x}, t' , and z_1 . The polar angle of the bremsstrahlung photon $\theta_\gamma^{*(C)}$ is measured with respect to the momentum of the incoming quark. Then

$$t'_{(C)}^\pm = t + E_\gamma^* (E_e^* - E_e^* - |\mathbf{p}_q^*| \cos \theta_\gamma^{*(C)\pm}) \quad (43)$$

and from $\Delta_4 \leq 0$ (for $m_f = 0$):

as a function of t' besides x, y, \hat{x} .

If the condition (38) does not restrict the angular integration and $\cos \theta_\gamma^{*(C)\pm} = \pm 1$ one has

$$t'_{(C)}^\pm = t + E_\gamma^* (E_e^* - E_e^* \pm |\mathbf{p}_e^* - \mathbf{p}_e^*|). \quad (45)$$

Using (1) one can express these limits as functions of x, y , and \hat{x} . Then it becomes obvious that the minimum of $|t'|$ is determined by the quark mass:

$$|t'|_{\min} = \frac{1}{\hat{x}(\hat{x}-x)} x^2 m_q^2 + \mathcal{O}(m_q^2/yS). \quad (46)$$

The lower limit for the $|t'|$ integration can also be calculated without relying on the parton model assumption

from the kinematics of ep scattering. Then $|t'|_{\min}$ is determined by the proton mass M_p :

$$|t'|_{\min} = \frac{\hat{x}}{\hat{x}-x} x^2 M_p^2 + \mathcal{O}(M_p^2/yS). \quad (47)$$

This could be obtained from (46) by substituting $m_q \rightarrow \hat{x}M_p$. For large x and small y the small $|t'|$ -region (i.e. the Compton part) is irrelevant and the different prescriptions (46) or (47) lead to negligible differences in the final results. The Compton contribution becomes increasingly important, however, for small x and large y and the results are sensitive then to the value chosen for m_q . Because of the additional factor $1/\hat{x}^2$ in (46) the prescription using a quark mass is, for small \hat{x} , equivalent to cutting off the $|t'|$ integration at larger values, if m_q is not chosen too small.

Acknowledgments. We thank A. Akhundov, D. Yu. Bardin, W. Krasny, and G. Schuler for helpful discussions. We appreciate also many helpful suggestions and the encouraging support of G. Kramer. A.K. and H.-J. M. thank for financial support from DESY.

References

1. D. Yu. Bardin, C. Burdik, P.Ch. Christova, T. Riemann: Dubna preprint E2-87-595, E2-88-682; Z. Phys. C – Particles and Fields 42 (1989) 679
2. M. Böhm, H. Spiesberger: Nucl. Phys. B294 (1987) 1081
3. H. Spiesberger: DESY-89-175, 13th International school of theoretical physics, Szczyrk, Poland, 1989
4. D. Yu. Bardin, C. Burdik, P.Ch. Christova, T. Riemann: Z. Phys. C – Particles and Fields 44 (1989) 149
5. M. Böhm, H. Spiesberger: Nucl. Phys. B304 (1987) 749
6. Proceedings of the HERA Workshop, Hamburg 1987, R.D. Peccei (ed), Vol. 2, p. 577
7. W. Beenakker, F.A. Berends, W.L. van Neerven: Proceedings of the Ringberg workshop on radiative corrections for e^+e^- collisions, Ringberg 1989, J.H. Kühn (ed.), p. 3
8. J. Blümlein: Z. Phys. C – Particles and Fields 47 (1990) 89
9. S. Jadach: MPI-PAE/PTh 75/86 (1986)
10. K.J.F. Gaemers, M. van der Horst: Nucl. Phys. B316 (1989) 289; Err. Nucl. Phys. B336 (1990) 184
11. H. Spiesberger: DESY 90-053, to appear in Nucl. Phys. B
12. A. Kwiatkowski, H.-J. Möhring, H. Spiesberger: DESY-90-041
13. V. Blobel: CERN-85-09, Proc. Aiguablava, CERN Comp. School 1984, 88
14. S. de Jong, J. Vermaseren: AXO User Manual, NIKHEF-H Report, Amsterdam 1987
15. G. Peter Lepage: J. Comput. Phys. 27 (1978) 192
16. A. Kwiatkowski: PhD thesis, in preparation
17. J. Feltesse: Proceedings of the HERA Workshop, Hamburg 1987, R.D. Peccei (ed.), Vol. 1, p. 33
18. J. Kripfganz, H.-J. Möhring, H. Spiesberger: Z. Phys. C – Particles and Fields 49 (1990) 501
19. A.A. Akhundov, D.Yu. Bardin, L.V. Kalinovskaja: DESY 90-130
20. J. Blümlein, G. Levman, H. Spiesberger: Proc. Snowmass 1990
21. D.W. Duke, J.F. Owens: Phys. Rev. D30 (1984) 49
22. W. Hollik: Fortschr. Phys. 38 (1990) 165
23. P.N. Harriman, A.D. Martin, W.J. Stirling, R.G. Roberts: Phys. Rev. D42 (1990) 798
24. S.V. Levonian et al.: H1-TR113 (1987)
25. S. Jadach, M. Jezabek, W. Płaczek: Phys. Lett. B248 (1990) 417